



An improved multiaxial rainflow algorithm for non-proportional stress or strain histories – Part I: Enclosing surface methods

Marco Antonio Meggiolaro*, Jaime Tupiassú Pinho de Castro

Department of Mechanical Engineering, Pontifical Catholic University of Rio de Janeiro, Rua Marquês de São Vicente 225 – Gávea, Rio de Janeiro, RJ 22453-900, Brazil

ARTICLE INFO

Article history:

Available online 7 November 2011

Keywords:

Rainflow algorithms
Multiaxial fatigue
Non-proportional loadings
Enclosing surface methods
Multiaxial

ABSTRACT

The objective of this work is to develop a simple multiaxial version of a rainflow algorithm that allows the proper calculation of multiaxial fatigue damage induced by non-proportional load histories. One of the issues in such algorithm involves a complementary problem, how to properly quantify equivalent stress or strain ranges and mean components associated with each rainflow-counted cycle. A traditional way to estimate such ranges is to use enclosing surface methods, which search for convex enclosures like balls or prisms, of the entire history path in stress or strain diagrams. To treat these two intrinsically related problems, this work is divided into two parts. Part I deals with how to compute equivalent stress or strain ranges in multiaxial NP histories using enclosing surface methods. The available methods are first reviewed, and new enclosing surface models are proposed, based on Deperrois' idea of longest chords. Then, these methods are compared using results from more than 3×10^6 Monte Carlo simulations of random and especially chosen path topologies in two to five-dimensional stress or strain diagrams. Moreover, a new simpler but powerful approach to evaluate equivalent stress and strain ranges in NP histories is presented, called the Moment Of Inertia (MOI) method. The MOI method is not based on enclosing surfaces, it assumes instead that the path contour in the stress or strain diagram is analogous to a homogeneous wire with a unit mass. The center of mass of such wire gives then the mean component of the path, while the moments of inertia of the wire can be used to obtain the equivalent stress or strain ranges. Experimental results for 15 different multiaxial histories prove the effectiveness of the MOI method to predict the associated fatigue lives, when compared to the existing enclosing surface methods. Part II of this paper presents a multiaxial rainflow counting algorithm that allows the MOI and enclosing surface methods to be generalized to non-periodic NP histories and to periodic NP histories formed by complex blocks with multiple cycles each.

© 2011 Elsevier Ltd. All rights reserved.

1. Introduction

Non-proportional (NP) multiaxial fatigue damage occurs when the principal stress directions vary during the loading induced by several independent sources, such as out-of-phase bending and torsion moments [1]. Uniaxial rainflow counting techniques cannot be applied to identify complex loading cycles or events in these cases, which require specific multiaxial counting routines. Besides, equivalent stress or strain ranges and mean components must be associated with each multiaxial rainflow-counted load event. These components are traditionally estimated by convex circular, ellipsoidal or prismatic enclosures of the entire history path in stress or strain diagrams. Besides the existing enclosing surface models, others can be proposed based on Deperrois' longest chords idea [2]. However, enclosing surface methods have a few limita-

tions that will be discussed in this work. To compensate for them, a new method is also proposed here, called the Moment Of Inertia (MOI) method, which is not based on path enclosures, which might be a better option to deal with such problems. Indeed, experimental results for 13 different multiaxial histories collected from comprehensive studies [3–4] prove the effectiveness of the MOI method to predict the associated fatigue lives, when compared to the existing enclosing surface methods, as discussed later on. But before doing so, it is important to review some multiaxial fatigue fundamentals.

Most multiaxial fatigue damage models are based on some stress or strain range, such as the octahedral shear stress range $\Delta\tau_{Mises}$ used in Sines [5] and Crossland [6] models; the shear stress range $\Delta\tau(\theta)$, projected onto a candidate plane defined by a given direction θ , used by Findley [7]; the maximum shear ranges $\Delta\tau_{max}$ from McDiarmid [8], and $\Delta\gamma_{max}$ used in Brown–Miller [9] and Fatemi–Socie [10] models; and the normal strain range $\Delta\varepsilon_{\perp}$ perpendicular to the crack plane, used in the Smith–Watson–Topper or SWT model [11]. It is not difficult to define these ranges for

* Corresponding author. Tel.: +55 21 3527 1424; fax: +55 21 3527 1165.

E-mail addresses: meggi@puc-rio.br (M.A. Meggiolaro), jtcastro@puc-rio.br (J.T.P. de Castro).

proportional constant amplitude loadings, where only two stress or strain states need to be considered, one associated with the load peaks and the other with its valleys.

However, for multiaxial variable amplitude (VA) loadings, in special when their histories are non-proportional (NP), it is not evident how these ranges should be defined and identified. Such complex loading paths, when represented e.g. in the Mises strain diagram $\varepsilon \times \gamma/\sqrt{3}$, can have a generic curved shape spanning infinitely many strain states, without any clear peak or valley. Indeed, peaks (or valleys) of one strain component may not (and generally do not) coincide with peaks (or valleys) of the other strain components [12]. One way to avoid such issues would be to use appropriate continuum damage models that include a variational formulation of the damage rate [13], since these models do not require the definition of load ranges. But no such model has been unquestionably accepted by the technical community yet – maybe because fatigue damage is a too localized and even directional phenomenon to be well described by continuum damage models. Anyway, the most popular fatigue damage models require the definition of a strain or stress range, as discussed above.

This first part of the paper deals with how to quantify the stress or strain ranges used by the various multiaxial fatigue damage models, associated with VA-NP histories that are periodic in time. Its Part II will then generalize these concepts for non-periodic VA-NP load histories, addressing multiaxial cycle counting issues and proposing new procedures to solve some problems faced by the available counting routines.

Consider a periodic load history formed by repeatedly following a given loading path domain D , where D contains all points from the stress or strain variations along one of its periods. The effective stress or strain ranges associated with D are usually more difficult to obtain than the mean values. For Findley's model [7], or for Case A cracks (Fig. 1) in McDiarmid's model [8], after projecting D onto a candidate plane perpendicular to the surface (i.e. with $\phi = 90^\circ$ from Fig. 1), the maximum shear stress variation $\Delta\tau_{max}$ is basically the difference between the maximum and minimum values along D of the shear stress τ_A that acts parallel both to the surface and to the critical plane. The approach is similar for strain-based methods: the shear strain range $\Delta\gamma_{max}$ or the normal strain range $\Delta\varepsilon_\perp$ are easy to obtain in Case A cracks, since the projected history only needs to deal with a single shear γ or normal ε_\perp strain component

(except for the Brown–Miller method [9], which uses both γ and ε_\perp components, however they are treated independently in the multi-channel rainflow count of [12]). On the other hand, the mean or maximum value of the normal stresses along each cycle can be directly obtained from the rainflow algorithm presented in [12].

For Case B cracks (Fig. 1), Brown–Miller's and SWT's $\Delta\varepsilon_\perp$ should be easy to obtain from the normal strain history perpendicular to each candidate plane. But the effective $\Delta\tau_{max}$ or $\Delta\gamma_{max}$ are not easy to define for Case B cracks, since a generic NP loading path D results in NP variations of both shear stresses τ_B and τ_{B2} that act parallel to the critical plane. As both τ_B and τ_{B2} influence the growth of Case B shear cracks along the critical plane, τ_{B2} should not be neglected. To calculate the maximum strain range $\Delta\tau_{max}$ at the critical plane considering τ_{B2} , it is necessary to draw the path D of the stress history along a $\tau_B \times \tau_{B2}$ diagram, as shown in Fig. 2.

For complex-shaped load histories, such as the relatively simple one shown in the figure, it is not easy to decide how to obtain the effective $\Delta\tau_{max}$. The search for an effective range using the deviatoric stress path started with the pioneering work of Dang Van [14], who studied various methods to define and calculate it. Since then, several "enclosing surface methods" have been proposed [15–19], which try to find circles, ellipses or rectangles that contain the entire load path (in the 2D case). In a nutshell, in the 2D case, the Minimum Ball (MB) method [15] searches for the circle with minimum radius that contains D ; the minimum ellipse methods [16–18] search for an ellipse with semi-axes a and b that contains D with minimum area πab or minimum norm $(a^2 + b^2)^{1/2}$; and the maximum prismatic hull methods [17,19] search among the smallest rectangles that contain D the one with maximum area or maximum diagonal (it's a max–min search problem). The value of $\Delta\tau_{max}$ in Fig. 2 would either be assumed as the value of the circle diameter, or twice the ellipse norm, or the length of the enclosing rectangle diagonal. If the history path was represented in a $\gamma_B \times \gamma_{B2}$ diagram, these exact same methods would result in estimates for $\Delta\gamma_{max}$.

The enclosing surface methods can also be applied to traction-torsion histories, if a $\sigma_x \times \tau_{xy}\sqrt{3}$ diagram is considered. The effective range in this case is the Mises stress range $\Delta\sigma_{Mises}$. Similarly, for traction-torsion histories where plastic strains dominate, a strain diagram $\varepsilon_x \times \gamma_{xy}/\sqrt{3}$ can be used to predict an effective Mises strain range $\Delta\varepsilon_{Mises}$.

Such enclosing surface methods can be extended to histories involving more than two stress or strain components. E.g., if the history path is plotted in a 3D diagram representing 3 stress or strain components, the enclosing surface methods will search for spheres, ellipsoids or rectangular prisms. For higher dimension

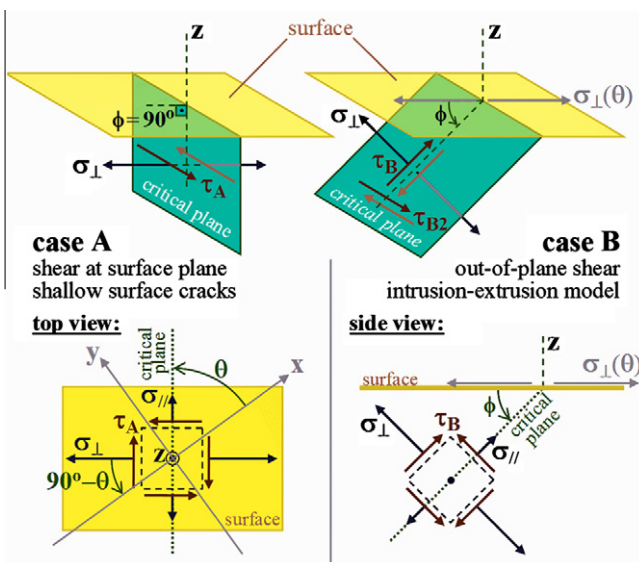


Fig. 1. Case A and Case B cracks.

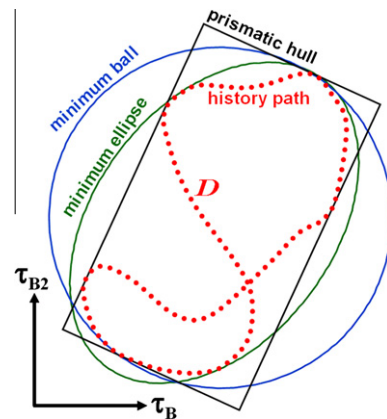


Fig. 2. Periodic (or single) stress history path D in the $\tau_B \times \tau_{B2}$ diagram, enclosed in surfaces such as circles (balls), ellipses and rectangular prisms.

diagrams, the search is for hyperspheres, hyperellipsoids, and rectangular hyperprisms. However, this practice can lead to significant errors, since each enclosing surface will reflect an effective range calculated on different planes at different points in time [1]. The recommended approach for general 6D histories involving all stress (or strain) components is the one proposed by Bannantine and Socie [1]: to project them onto Cases A and B candidate planes, resulting for the Case B planes in searches for effective ranges in 2D diagrams $\tau_B \times \tau_{B2}$ or $\gamma_B \times \gamma_{B2}$.

The existing enclosing surface methods are described in the following section. Their framework is based on deviatoric stress (or strain) diagrams and Mises stress (or strain) parameters, which are discussed next.

2. Mises stress and strain parameters

The methods to obtain effective (or equivalent) stress and strain ranges usually make use of stress and strain parameters based on the Mises yield function. For linear elastic histories, both Mises effective stress σ_{Mises} and Mises shear stress τ_{Mises} can be used as auxiliary parameters, where

$$\begin{aligned} \sigma_{Mises} &= \frac{3}{\sqrt{2}} \tau_{Mises} \\ &= \frac{1}{\sqrt{2}} \\ &\quad \times \sqrt{(\sigma_x - \sigma_y)^2 + (\sigma_y - \sigma_z)^2 + (\sigma_x - \sigma_z)^2 + 6(\tau_{xy}^2 + \tau_{yz}^2 + \tau_{xz}^2)} \end{aligned} \quad (1)$$

Since the σ_{Mises} equation is always positive, a Mises stress range $\Delta\sigma_{Mises}$ (also known as relative Mises stress σ_{RMises}) should be used to correctly evaluate the variation of σ_{Mises} due to a change $(\Delta\sigma_x, \Delta\sigma_y, \Delta\sigma_z, \Delta\tau_{xy}, \Delta\tau_{xz}, \Delta\tau_{yz})$ in the stress components along some loading path:

$$\begin{aligned} \Delta\sigma_{Mises} &= \sigma_{RMises} \\ &= \frac{\sqrt{(\Delta\sigma_x - \Delta\sigma_y)^2 + (\Delta\sigma_x - \Delta\sigma_z)^2 + (\Delta\sigma_y - \Delta\sigma_z)^2 + 6(\Delta\tau_{xy}^2 + \Delta\tau_{xz}^2 + \Delta\tau_{yz}^2)}}{\sqrt{2}} \end{aligned} \quad (2)$$

Note that the Mises stress range correlates with the shear range parameter $\Delta\tau_{Mises}$, used in both Sines and Crossland multiaxial fatigue damage models, through $\Delta\sigma_{Mises} = \Delta\tau_{Mises} \cdot 3/\sqrt{2}$

The Mises effective strain ε_{Mises} is another useful quantity in VA-NP histories, in special to deal with plastic strains. It uses the mean or effective Poisson coefficient $\bar{\nu} = (0.5\varepsilon_{pl} + \nu_{el}\varepsilon_{el})/(\varepsilon_{pl} + \varepsilon_{el})$ to consider plastic effects, where ε_{el} and ε_{pl} are the elastic and plastic components of the strains, and ν_{el} and ν_{pl} are the elastic and plastic Poisson coefficients (where $\nu_{pl} \cong 0.5$). The Mises strain correlates with the Mises shear strain γ_{Mises} , which is the combination of both shear strains that act in each of the octahedral planes, through

$$\begin{aligned} \varepsilon_{Mises} &= \frac{3}{2\sqrt{2} \cdot (1 + \bar{\nu})} \gamma_{Mises} \\ &= \frac{\sqrt{(\varepsilon_x - \varepsilon_y)^2 + (\varepsilon_x - \varepsilon_z)^2 + (\varepsilon_y - \varepsilon_z)^2 + 1.5(\gamma_{xy}^2 + \gamma_{xz}^2 + \gamma_{yz}^2)}}{\sqrt{2} \cdot (1 + \bar{\nu})} \end{aligned} \quad (3)$$

Since the ε_{Mises} equation is always positive, a Mises strain range $\Delta\varepsilon_{Mises}$ (also known as the relative Mises strain ε_{RMises}) should be used to evaluate its variation due to any change in the strain components $(\Delta\varepsilon_x, \Delta\varepsilon_y, \Delta\varepsilon_z, \Delta\gamma_{xy}, \Delta\gamma_{xz}, \Delta\gamma_{yz})$ along some loading path:

$$\begin{aligned} \Delta\varepsilon_{Mises} &= \varepsilon_{RMises} \\ &= \frac{\sqrt{(\Delta\varepsilon_x - \Delta\varepsilon_y)^2 + (\Delta\varepsilon_x - \Delta\varepsilon_z)^2 + (\Delta\varepsilon_y - \Delta\varepsilon_z)^2 + 1.5(\Delta\gamma_{xy}^2 + \Delta\gamma_{xz}^2 + \Delta\gamma_{yz}^2)}}{\sqrt{2} \cdot (1 + \bar{\nu})} \end{aligned} \quad (4)$$

A range parameter $\Delta\gamma_{Mises}$ can also be defined, related to the Mises strain range by

$$\Delta\varepsilon_{Mises} = \frac{3 \cdot \Delta\gamma_{Mises}}{2\sqrt{2}(1 + \bar{\nu})} \quad (5)$$

Note that since the shear stress or strain ranges $\Delta\tau_{Mises}$ or $\Delta\gamma_{Mises}$ are measured on the octahedral planes, they are not equal to twice the shear amplitudes τ_a or γ_a acting on the considered plane. But those shear amplitudes could be easily obtained by

$$\begin{aligned} \tau_a &= \frac{\sqrt{6}}{4} \Delta\tau_{Mises} = \frac{\sqrt{3}}{6} \Delta\sigma_{Mises} \text{ and } \gamma_a = \frac{\sqrt{3}}{6} \Delta\gamma_{Mises} \\ &= \frac{1 + \bar{\nu}}{\sqrt{3}} \Delta\varepsilon_{Mises} \end{aligned} \quad (6)$$

Finally, for the linear elastic case (where $\bar{\nu} = \nu_{el}$), all these relative Mises stresses and strains correlate with the Mises shear range parameters by

$$\Delta\sigma_{Mises} = E \cdot \Delta\varepsilon_{Mises} = \frac{3}{\sqrt{2}} \cdot \Delta\tau_{Mises} = \frac{3E}{2\sqrt{2} \cdot (1 + \nu_{el})} \cdot \Delta\gamma_{Mises} \quad (7)$$

When dealing with incremental plasticity problems, it is convenient to represent the stresses or strains in a 9-dimensional (9D) space instead of a 6D space [20]. But, to find effective ranges in VA-NP histories, it is a good idea to work in a space with reduced 6D dimensions. Moreover, since the deviatoric stresses S_x, S_y and S_z are linear-dependent, because $S_x + S_y + S_z = 0$, it is possible to reduce the deviatoric stress dimension from the 6D representation to 5D [21]. In this paper, the transformation proposed by Papadopoulos et al. [22] is used to obtain a reduced-order deviatoric stress tensor S' represented in a 5D transformed Euclidean stress-space $E_{5\sigma}$, where

$$\begin{cases} \bar{S}' \equiv [S_1 \ S_2 \ S_3 \ S_4 \ S_5]^T \\ S_1 \equiv \sigma_x - \frac{\sigma_y}{2} - \frac{\sigma_z}{2} = \frac{3}{2} S_x, S_2 \equiv \frac{\sigma_y - \sigma_z}{2} \sqrt{3} = \frac{S_y - S_z}{2} \sqrt{3} \\ S_3 \equiv \tau_{xy} \sqrt{3}, S_4 \equiv \tau_{xz} \sqrt{3}, S_5 \equiv \tau_{yz} \sqrt{3} \end{cases} \quad (8)$$

For strain histories, a similar transformation to a 5D transformed Euclidean strain-space $E_{5\varepsilon}$ is used for the deviatoric strains, resulting in a reduced-order deviatoric strain $\bar{\varepsilon}'$ represented by

$$\begin{cases} \bar{\varepsilon}' \equiv [e_1 \ e_2 \ e_3 \ e_4 \ e_5]^T \\ e_1 \equiv \frac{3}{2} \cdot \frac{\varepsilon_x}{1 + \bar{\nu}} = \frac{2\varepsilon_x - \varepsilon_y - \varepsilon_z}{2 \cdot (1 + \bar{\nu})}, e_2 \equiv \frac{\varepsilon_y - \varepsilon_z}{2 \cdot (1 + \bar{\nu})} \sqrt{3} = \frac{\varepsilon_y - \varepsilon_z}{2 \cdot (1 + \bar{\nu})} \sqrt{3}, \\ e_3 \equiv \frac{\gamma_{xy} \sqrt{3}}{2 \cdot (1 + \bar{\nu})}, e_4 \equiv \frac{\gamma_{xz} \sqrt{3}}{2 \cdot (1 + \bar{\nu})}, e_5 \equiv \frac{\gamma_{yz} \sqrt{3}}{2 \cdot (1 + \bar{\nu})} \end{cases} \quad (9)$$

where $\bar{\nu}$ is the effective Poisson coefficient. Note that the norms of \bar{S}' and $\bar{\varepsilon}'$ are equal to the Mises equivalent stress σ_{Mises} and strain ε_{Mises} .

After defining all involved stress and strain parameters, the enclosing surface methods are discussed. These methods are based on surfaces that enclose the history path in the above defined stress or strain sub-spaces. There are three main types of enclosing surfaces: balls, ellipsoids and rectangular prisms, reviewed next.

3. Enclosing Surface Methods

In his pioneer work, Dang Van [14,15] realized that the search for an effective stress range must take place on the deviatoric stress space. For periodic elastic histories, the mesoscopic stresses and strains in the critically oriented grain should stabilize by the

process of elastic shakedown, generating a local residual stress at such critical grain, called a backstress. The location of such backstress in the deviatoric space can be estimated as the center of the Minimum Ball (MB) that encloses the history, i.e. the smallest circle, sphere or hypersphere that circumscribes the loading path. In Dang Van's method, each mesoscopic stress state along the history path is then compared to a limiting stress level to predict infinite life. However, this approach is not useful to calculate finite fatigue lives, since it does not deal with stress (or strain) ranges, only with individual stress states.

But the same MB circumscribed to the macroscopic history can be used to estimate an effective Mises stress range $\Delta\sigma_{Mises}$ (or strain range $\Delta\varepsilon_{Mises}$) to predict finite lives. The diameter d of such MB in the transformed deviatoric stress-space $E_{5\sigma}$ or strain-space $E_{5\varepsilon}$ (or in a 2D, 3D or 4D sub-space of such spaces) is the magnitude of the variation $\Delta\bar{S}$ (or $\Delta\bar{\varepsilon}$), which is equal to $\Delta\sigma_{Mises}$ (or $\Delta\varepsilon_{Mises}$). Therefore, the effective shear ranges $\Delta\tau_{max}$ (used in the Findley and McDiarmid models) and $\Delta\gamma_{max}$ (used in the Brown-Miller and Fatemi–Socie models), Mises ranges $\Delta\sigma_{Mises}$ and $\Delta\varepsilon_{Mises}$, and shear ranges $\Delta\tau_{Mises}$ (used in the Sines and Crossland models) and $\Delta\gamma_{Mises}$, can all be estimated from d using the MB method by

$$\begin{aligned}\Delta\sigma_{Mises} &= 3 \cdot \Delta\tau_{Mises}/\sqrt{2} = \Delta\tau_{max}\sqrt{3} = (2\tau_a) \cdot \sqrt{3} = |\Delta\bar{S}| = d \equiv L \cdot \lambda_{MB} \text{ or} \\ \Delta\varepsilon_{Mises} &= 3 \cdot \frac{\Delta\gamma_{Mises}}{2\sqrt{2}(1+\bar{\nu})} = \frac{\Delta\gamma_{max}\sqrt{3}}{2(1+\bar{\nu})} = \frac{(2\gamma_a) \cdot \sqrt{3}}{2(1+\bar{\nu})} = |\Delta\bar{\varepsilon}| = d \equiv L \cdot \lambda_{MB}\end{aligned}\quad (10)$$

where L is the longest chord in the history (the maximum Euclidean distance in the transformed space between any two points along the history path, measured in either stress or strain units) and λ_{MB} is a dimensionless parameter defined as the ratio between the Mises stress or strain range and L .

In the 2D case, if any two points from the history define the diameter of a circle that contains the entire path, then their distance L is equal to the diameter d , therefore $\lambda_{MB} = 1.0$. A noTable 2D case is for a path forming an equilateral triangle, where $\lambda_{MB} = 2/\sqrt{3} \cong 1.155$. For any other 2D path, it is found that $1.0 \leq \lambda_{MB} \leq 1.155$.

But the Minimum Ball (MB) method is not efficient to represent the behavior of NP histories. For instance, it would predict the same Mises ranges for a NP 90° out-of-phase circular path and a proportional path defined by a diameter of this circle, both resulting in $\lambda_{MB} = 1.0$. But a higher value of λ would certainly be expected for the NP history.

To solve this problem, Freitas et al. [16] proposed the Minimum Circumscribed Ellipsoid (MCE) method. It searches for an ellipse (or ellipsoid or hyperellipsoid, for higher dimensions) that circumscribes the entire history, with its longest semi-axis a_1 equal to the radius of the minimum ball, and with the smallest possible values for the remaining semi-axes a_i ($i > 1$). The Mises ranges are then

$$\Delta\sigma_{Mises} \text{ or } \Delta\varepsilon_{Mises} = 2 \cdot \sqrt{\sum_{i=1}^{dim} a_i^2} \equiv 2 \cdot F \quad (11)$$

where dim is the dimension of the history path, $2 \leq dim \leq 5$, and F is defined as the Frobenius norm of the ellipsoid, which is equal to the square root of the sum of the squares of the ellipsoid semi-axes. Here, the Frobenius norm is essentially an Euclidean distance (or Euclidean norm) between the origin and a point with coordinates $(a_1, a_2, \dots, a_{dim})$, since the axes of the reduced stress (or strain) space are orthonormal. In the case of tensors, the Euclidean norm is commonly called the Frobenius norm, usually abbreviated as F -norm [18].

The ratio λ_{MCE} between the Mises ranges calculated by the MCE method and the longest chord L reproduces experimental data bet-

ter than λ_{MB} (generated by the MB method). In the 2D case, a NP circular path would result in $\lambda_{MCE} = \sqrt{2}$ instead of the proportional value 1.0, which is much more reasonable than the MB prediction. It is also found that any 2D path results in $1.0 \leq \lambda_{MCE} \leq \sqrt{2}$, with the maximum value occurring e.g. for circular and square paths. In general, for any dimension dim , it is found that $1.0 \leq \lambda_{MCE} \leq \sqrt{dim}$, with the maximum value \sqrt{dim} occurring e.g. for paths that follow the edges of hypercubes or large portions of the surface of hyperspheres.

The downside of the MCE method is the requirement that the longest semi-axis must be equal to the radius of the Minimum Ball. E.g., a very elongated (almost proportional) rectangular path would give a circle as the MCE. The MCE would thus predict $\lambda_{MCE} = \sqrt{2}$ for an almost proportional rectangular path, instead of the expected value of 1.0.

A possible alternative to the MCE method is to search for the Minimum Volume Ellipsoid (MVE), also known as the Löwner–John Ellipsoid. In the 2D case, it is basically the search for an enclosing ellipse with minimum area. Such MVE method solves the issue with rectangular paths discussed above, however it tends to find ellipses with lower aspect ratios than expected.

Another alternative to the MCE method is the search for the Minimum F -norm Ellipsoid (MFE) [17]. Instead of searching for the minimum volume (or area), the MFE looks for the ellipse, ellipsoid, or hyperellipsoid with minimum value of its F -norm F , defined in Eq. (11). Zouain et al. [18] present an efficient (although computationally intensive) method to numerically find such MFE. Other efficient algorithms can be found in [23].

The ratios between the Mises stress or strain ranges $2F$ calculated from the MCE, MVE and MFE methods and the longest chord L are defined, respectively, as λ_{MCE} , λ_{MVE} and λ_{MFE} . All these ratios must be greater than or equal to 1.0. In the 2D case, a notable path is the one with the shape of an equilateral triangle with sides L (which are also its longest chords), where the enclosing surface is a circle with diameter $d = 2L/\sqrt{3}$ and F -norm $F = d\sqrt{2}$, resulting in $\lambda_{MCE} = \lambda_{MVE} = \lambda_{MFE} = 2 \cdot F/L = 2\sqrt{2}/\sqrt{3} \cong 1.633$. For any other 2D path, it is found that $1.0 \leq \lambda_{MCE} \leq 1.633$ and $1.0 \leq \lambda_{MFE} \leq 1.633$. On the other hand, λ_{MVE} can reach values beyond 2.0 when a very elongated enclosing ellipse is the solution with minimum area, an indication that the MVE method can be very conservative.

Another class of enclosing surface methods tries to find a rectangular prism with sides $2a_1, \dots, 2a_{dim}$ that encloses a load history path, where dim is the dimension of the considered space. There are essentially four methods to fit rectangular prisms to the history path.

The first is the Maximum Prismatic Hull (MPH). This method searches for the smallest rectangular prism that encloses the history (the minimum prism), for each possible orientation (of the prism). Among them, the one with highest F -norm is chosen. The F -norm and resulting Mises ranges are the same defined in Eq. (11), except that here a_i are the semi-lengths (half the length) of the rectangular prism sides. The MPH was originally proposed by Gonçalves et al. in [17] for sinusoidal time histories, and later extended by Mamiya et al. in [19] for a general NP loading.

Another prismatic hull method is the Maximum Volume Prismatic Hull (MVPH), which searches among the minimum prisms the one with maximum volume. Although the search is for a maximum volume, the F -norm is also used to compute the Mises range. In the 2D case, the MVPH method is essentially the search, among the minimum rectangles that enclose the entire path, of the one with maximum area (it's a max–min problem).

A third method is proposed here, called the Maximum Prismatic Hull with Longest Chords (MPHLC). It is basically an improvement of Deperrois' longest chord method [2], which provides satisfactory results [24]. However, Papadopoulos [22] criticizes it because, if

any longest chord is non-unique, then different rectangular prisms and resulting shear amplitudes could be obtained for the same history. But this non-uniqueness could be easily solved by stating that, when the longest chords are non-unique, then the chosen prismatic hull would be the one with maximum F-norm among all possible results. The use of rectangular prisms with maximum F-norm has shown good results in the MPH method, therefore this could be the solution to Papadopoulos' criticisms. The combination of the MPH and Deperrois' methods thus leads to the MPHLC method, performed in 4 steps:

- (1) define the longest side $2a_1$ of the rectangular prism in the direction of the longest chord L of the history;
- (2) project the history into the sub-space orthogonal to the directions of all sides of the prisms that have already been defined (for a history with dimension dim , if m sides have already been chosen, then such sub-space will have $dim-m$ dimensions);
- (3) define the next side $2a_i$ of the rectangular prism in the direction of the longest chord measured in the projected sub-space, and repeat step 2 until all sides are found;
- (4) if multiple solutions for the rectangular prism are found, the one with maximum F-norm is chosen – this step addresses Papadopoulos' criticisms [22].

The advantage of the MPHLC method over the MPH or MVPH is that it does not require a numerical search for the prismatic hull orientation. Its orientation is deterministically defined by the longest chords.

A variation of the MPHLC is also proposed, called the Maximum Prismatic Hull with Container Chords (MPHCC). It is similar to the MPHLC, but all chords that contain the orthogonal projection of the entire history onto them (called here "container chords") are considered as candidate directions for the sides of the rectangular prism. Note that every longest chord LC is a "container chord" CC, but not every CC is a LC. From the probable multiple solutions for the resulting rectangular prisms, the one with maximum F-norm is chosen.

The ratios between the Mises stress or strain ranges $2F$ calculated from the MPH, MVPH, MPHLC and MPHCC methods and the longest chord L are defined, respectively, as λ_{MPH} , λ_{MVPH} , λ_{MPHLC} and λ_{MPHCC} .

In summary, enclosing surface methods can be useful to estimate the equivalent stress (or strain) amplitude associated with NP loading paths. However, such methods have three issues. First of all, among all enclosing surface methods, only the MB has a physical foundation. The search of the minimum ball enclosing a history path in the deviatoric space corresponds to the search of the elastic-shakedown state that the material grains in the neighbour of the point of interest could attain under periodic loading, considering an isotropic and/or kinematic hardening behavior [1]. In other words, fracture by fatigue is avoided if an elastic shakedown state can be reached. On the other hand, the enclosing ellipsoids and prisms are not derived from physical considerations, they are empirical methods that try to interpolate the limit cases between a proportional loading and a highly non-proportional one. Even so, these methods still have their practical value as engineering tools for relatively simple loading paths, as long as their effectiveness is experimentally verified.

The second issue is that each portion of the considered path should not involve more than 1 cycle. Otherwise, if it is considered as a single cycle, the actual damage might be underestimated. Instead, a multiaxial rainflow algorithm should be applied to the entire stress or strain history, and then an enclosing surface method should be applied for the path of each rainflow-counted reversal. This second issue will be addressed in Part II of this paper.

Finally, the third issue involves information loss. Enclosing surface algorithms do not take into account the actual loading path, but only the convex hulls associated with them. For instance, consider a square path ABCD in a 2D deviatoric space. The convex hull of such path, defined as the convex enclosure with minimum area that contains the entire path, is the square itself. An hourglass-shaped path ABDC or ADBC would have the same convex hull: the square ABCD. It is not difficult to prove that the enclosing circle, ellipse or prismatic hull from any presented method would result in the same enclosure for these three considered paths, treating them as identical. In general, all paths that share the same convex hull share as well the same enclosing surface for a given method, even though they might lead to different equivalent amplitudes and fatigue lives. This third issue is addressed by a novel method to calculate equivalent and mean components that takes into account the actual loading path, not only its convex hull. This new method is presented next.

4. The Moment Of Inertia (MOI) method

The Moment Of Inertia (MOI) method is proposed here to calculate alternate and mean components of complex NP load histories. To accomplish that, the history must first be represented in a 2D subspace of the transformed 5D Euclidean stress-space $E_{5\sigma}$ (for stress histories) or $E_{5\epsilon}$ (for strain histories). The MOI method assumes that the 2D path/domain D , represented by a series of points (X, Y) from the stress or strain variations along it, is analogous to a homogeneous wire with unit mass. Note that X and Y can have stress or strain units, but they are completely unrelated to the directions x and y usually associated with the material surface. The mean component of D is assumed, in the MOI method, to be located at the center of gravity of this imaginary homogeneous wire shaped as the history path. Such center of gravity is located at the perimeter centroid (X_c, Y_c) of D , calculated from contour integrals along the entire path

$$X_c = \frac{1}{p} \cdot \oint X \cdot dp, \quad Y_c = \frac{1}{p} \cdot \oint Y \cdot dp, \quad p = \oint dp \quad (12)$$

where dp is the length of an infinitesimal arc of the path and p is the path perimeter, see Fig. 3.

The MOI method is so called because it makes use of the mass moments of inertia (MOI) of such homogeneous wire. These moments are first calculated with respect to the origin O of the diagram, assuming the wire has unit mass, resulting in

$$\begin{aligned} I_{XX}^O &= \frac{1}{p} \cdot \oint Y^2 \cdot dp, & I_{YY}^O &= \frac{1}{p} \cdot \oint X^2 \cdot dp, & I_{XY}^O &= \\ &= -\frac{1}{p} \cdot \oint X \cdot Y \cdot dp \end{aligned} \quad (13)$$

Then, the mass moments of inertia of such unit mass wire, with respect to its center of gravity (X_c, Y_c) , are obtained. They are computed from the moments of inertia of the path D with respect to its perimeter centroid (X_c, Y_c) , which are easily obtained from the parallel axis theorem, assuming a unit mass:

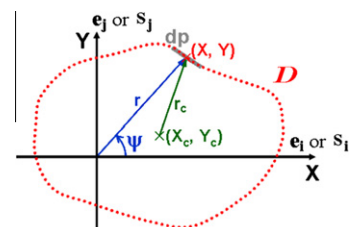


Fig. 3. Load history path, assumed as a homogeneous wire with unit mass in the deviatoric 2D space.

$$I_{XX} = I_{XX}^0 - Y_c^2, \quad I_{YY} = I_{YY}^0 - X_c^2, \quad I_{XY} = I_{XY}^0 + X_c \cdot Y_c \quad (14)$$

The MOI method assumes that the deviatoric stress or strain ranges, $\Delta S \equiv \Delta \sigma_{Mises}$ or $\Delta e \equiv \Delta \varepsilon_{Mises}$, depend on the mass moment of inertia I_{ZZ} with respect to the perimeter centroid, perpendicular to the X - Y plane. This is physically sound, since history paths further away from their perimeter centroid PC will contribute more to the effective range and amplitude, which is coherent with the fact that wire segments further away from the center of gravity of an imaginary homogeneous wire contribute more to its MOI. Note that the use of integral parameters to evaluate NP paths is not new, it was already used e.g. in [3] to estimate the non-proportionality factor. But the use of a moment of inertia analogy to obtain effective ranges is a novel idea, a true alternative for the enclosing surface methods discussed above.

From the perpendicular axis theorem, which states that $I_{ZZ} = I_{XX} + I_{YY}$, and from a dimensional analysis, it is found that

$$\frac{\Delta \sigma_{Mises}}{2} \text{ or } \frac{\Delta \varepsilon_{Mises}}{2} = \sqrt{3 \cdot I_{ZZ}} = \sqrt{3 \cdot (I_{XX} + I_{YY})} \quad (15)$$

The factor $\sqrt{3}$ is introduced to guarantee that a proportional loading path, represented by a straight segment with length L , perimeter $2L$ and unit mass $m = 1$, will result in the expected range $\Delta \sigma_{Mises}$ or $\Delta \varepsilon_{Mises}$ equal to L (since the MOI of a straight wire with respect to its centroid is $mL^2/12$).

Note that the above definitions are coherent, since they are independent of the X - Y system orientation because $I_{XX} + I_{YY}$ is an invariant, equal to the sum of the principal MOI $I_1 + I_2$ of the homogeneous wire which represents the loading path.

The MOI method is simple to calculate, in special for polygonal histories. The mass moments of inertia of curved histories are also easy to calculate from fine polygonal discretizations. In addition, the MOI method can make use of classical mass moment of inertia tables, or even CAD programs applied to arbitrarily-shaped homogeneous wires, to calculate I_{XX} , I_{YY} , I_{XY} and I_{ZZ} .

To use the MOI approach in polygonal load history paths, it is enough to combine the expression for the moment of inertia of an inclined straight wire and the parallel axis theorem. If each side i of the polygon has length Δp_i , centered at (X_{ci}, Y_{ci}) , and making an angle ψ_i with respect to the horizontal (see Fig. 4), then the load path perimeter centroid PC and the MOI expressions with respect to the origin are obtained from

$$p = \sum_i \Delta p_i, \quad X_c = \frac{1}{p} \cdot \sum_i X_{ci} \cdot \Delta p_i, \quad Y_c = \frac{1}{p} \cdot \sum_i Y_{ci} \cdot \Delta p_i$$

$$I_{XX}^0 = \frac{1}{p} \cdot \sum_i \left(\frac{\Delta p_i^2}{12} \sin^2 \psi_i + Y_{ci}^2 \right) \cdot \Delta p_i, \quad I_{YY}^0 = \frac{1}{p} \cdot \sum_i \left(\frac{\Delta p_i^2}{12} \cos^2 \psi_i + X_{ci}^2 \right) \cdot \Delta p_i,$$

$$I_{XY}^0 = -\frac{1}{p} \cdot \sum_i \left(\frac{\Delta p_i^2}{12} \sin \psi_i \cos \psi_i + X_{ci} Y_{ci} \right) \cdot \Delta p_i \quad (16)$$

The MOI with respect to the load path PC is then calculated from Eq. (14).

Note that, similarly to the enclosing surface methods, the MOI method should only be applied to 2D histories. It would lead to significant errors if directly applied to 3D, 4D or 5D load histories, because the MOI method would be calculated on different planes at different points in time [1]. Instead, any 3D, 4D or 5D load history in the deviatoric space should first be projected onto a suitable candidate plane for the fatigue damage analysis. Then, for Case B cracks (Fig. 1), the history of the two shear stresses (or strains) acting parallel to the crack plane should be represented in a 2D diagram, where the MOI method would be applied.

In the next section, all presented methods are compared.

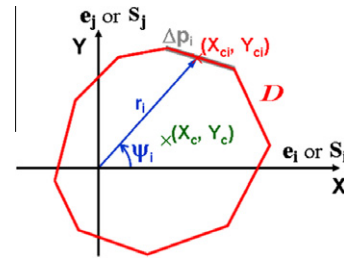


Fig. 4. Application of the MOI method to polygonal history paths.

5. Comparison among the enclosing surface methods

Fig. 5 shows the enclosing surfaces obtained from all presented methods for a rectangular history path in a reduced 2D sub-space, along with their ratios λ between the Mises ranges and longest chord L . Note that, in this example, L is the diagonal of the rectangular path.

Experimental results suggest that the expected Mises to longest chord ratio λ in this example is about 1.3. However, the Minimum Ball MB method predicts $\lambda_{MB} = 1.0$, a very non-conservative value. The MB assumes that such rectangular path would have the same Mises range L as a straight path along one of its diagonals, which is not reasonable. The Minimum Circumscribed Ellipsoid MCE method, on the other hand, overestimates λ , obtaining $\lambda_{MCE} = \sqrt{2} \cong 1.414$. The MCE method finds the same circle from the MB method to enclose such history, even though the aspect ratio of this rectangular path is very different from 1.0, which would suggest instead the use of an elongated elliptic hull.

The Minimum Volume Ellipsoid MVE method also tends to overestimate λ , obtaining in this example $\lambda_{MVE} = 1.413$. In the search for the minimum area (or volume, for higher dimension diagrams), the MVE method ends up finding overly elongated ellipses (with semi-axes $b \ll a$), which have a small area πab due to the very low value of b , but an unrealistically high F -norm $(a^2 + b^2)^{1/2}$ due to the high value obtained for a . Thus, λ_{MVE} overestimates the ratio λ , since it is calculated from this unrealistic value of the F -norm, and not from the minimized area (or volume).

Among the ellipsoid surface methods, the Minimum F -norm Ellipsoid MFE gives the best predictions, resulting in $\lambda_{MFE} = 1.295$,

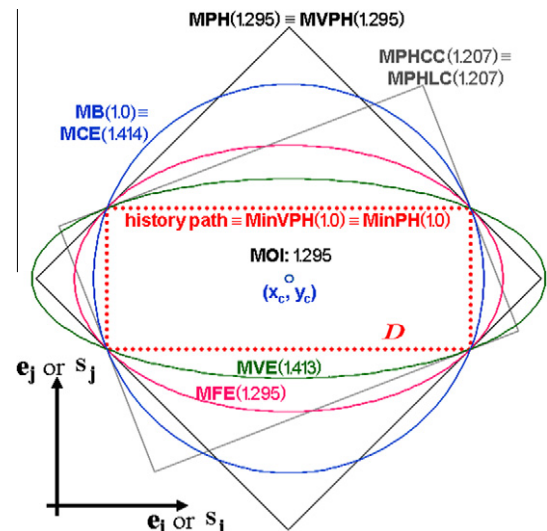


Fig. 5. Values of the Mises stress or strain range ratio λ for the MB, MCE, MVE, MFE, MPH, MPHLC, MPHCC, MVPH, MinVPH and MOI methods for a rectangular 2D history path.

with an enclosing ellipse with a much more reasonable aspect ratio than the ones from the MCE and MVE methods, see Fig. 5.

Both Maximum Prismatic Hull MPH and Maximum Volume Prismatic Hull MVPH methods obtain in this example $\lambda_{MPH} = \lambda_{MVPH} = 1.295$, which exactly agrees with the MFE prediction. Note, however, that the MPH and MFE methods are not equivalent, since they result in slightly different λ values between them for other history paths, as shown in [25].

The Maximum Prismatic Hull with Longest Chords MPHLC and Maximum Prismatic Hull with Container Chords MPHCC methods result in $\lambda_{MPHLC} = \lambda_{MPHCC} = 1.207$, a value about 7% lower than the MPH prediction. The fact that $\lambda_{MPHLC} \leq \lambda_{MPH}$ and $\lambda_{MPHCC} \leq \lambda_{MPH}$ is not a surprise, since the MPH searches for the maximum F-norm checking rectangles (in the 2D case) in all directions, while the MPHLC and MPHCC only search for rectangles in the directions of the longest and/or container chords. If these directions of longest or container chords coincide with the ones associated with a maximum F-norm rectangle (which is quite often true), then the MPHLC or MPHCC predictions will coincide with λ_{MPH} , otherwise they will result in λ ratios slightly lower than the upper bound λ_{MPH} .

Fig. 5 also shows the prismatic hulls MinPH and MinVPH with minimum (instead of maximum) F-norm and volume (or area, in 2D), respectively. In this example, these rectangular hulls would coincide with the original rectangular path, wrongfully predicting $\lambda = 1$. This counter-example shows why no prismatic hull method with minimum F-norm or volume has been proposed.

In summary, the MB method tends to underestimate the Mises stress or strain range ratio λ , while the MCE and MVE overestimate it. The MPHLC and MPHCC slightly underestimate λ , while the MFE, MPH and MVPH give very similar (although, in general, different) predictions, which agree with experimental results and with the MOI method prediction $\lambda_{MOI} = 1.295$, where λ_{MOI} is defined as the ratio between the MOI-calculated Mises stress or strain range and the longest chord L .

But the above considerations are based on a single simple example. To really compare all enclosing surface methods, it is necessary to study all possible history path topologies in 2D, 3D, 4D and 5D deviatoric stress or strain spaces. In this work, Monte Carlo simulations are performed for 3×10^6 2D history paths, 10^5 paths in 3D, 10^4 in 4D and 10^3 in 5D, including both random and especially selected paths to try to cover all possible path topologies. All enclosing surface methods are applied to each of these simulated paths, to evaluate and compare their λ predictions.

The random paths in 2D are selected as follows. Since the convex hull of a non-convex path has exactly the same enclosing surface of the path itself (for each and every considered method), it is enough to use only convex paths in the simulations, without generating biased statistics due to important path types that might have been disregarded. Note that the MOI method is not simulated here, otherwise non-convex paths would need to be considered as well, because this method is path-dependent. But to evaluate only convex enclosing surface methods, simulated non-convex paths are not necessary, since they're well described by the (convex) path along their convex hull perimeter.

Without loss of generality, a unit length segment is created in the horizontal direction and considered as the longest edge of the path. Then, 2×10^6 random convex quadrilaterals are uniquely defined from drawing random lengths between 0 and 1 for the next two edges, and random angles between 0 and 180 degrees for the next two internal angles. The remaining 10^6 random paths are drawn in a similar way, but for convex polygons with increasing number of sides. Since any convex path can be approximated by a convex polygon with a sufficient number of sides, the simulation could be considered as representative of any convex 2D path.

Interestingly, it was found that the quadrilateral paths were able to capture all relevant issues of the studied methods. Notable 2D paths in all method comparisons were the ones shaped as a square, an equilateral triangle, and a straight line (proportional path), all of which are a special or degenerate case of a quadrilateral. The polygonal paths with higher number of sides contributed to points that were almost invariably inside the point cloud from the quadrilateral simulations, see e.g. Fig. 6. Even the notable circular path, which required polygons with several sides to be well approximated, did not contribute much to the analysis, since its enclosing surface from each considered method is the same as the one for the already simulated square path.

A similar approach was performed for the 3D, 4D and 5D simulations, drawing random polygonal paths with increasing number of sides in such dimensions. Instead of using internal angles, the polygonal edges were defined from random 3D, 4D and 5D vectors with norms between 0 and 1.

One of the main challenges of these simulations was the need to implement the search algorithms for all existing enclosing surface methods. The details on the implemented search algorithms are beyond the scope of this work, but a few methods can be found in [25]. Note that fewer simulations are performed as the dimension increases, because of computing time restrictions, since most enclosing surface methods are very computationally intensive in higher dimensions. E.g., the search for the direction of a 5D hyperprism in the MPH method involves a search in a 10-dimensional space for the 10 angles that define its 5D orientation, which can be computationally intensive even for rough discretizations of each angle at 15° steps. On the other hand, the MPHLC and MPHCC methods are straightforward, deterministic (no numerical search method based on discretizations is required) and several orders of magnitude faster for higher dimension histories.

Table 1 shows the median values of the ratio between the λ ratios from each pair of enclosing surface methods, estimated from the Monte Carlo simulations for 2D paths, along with the associated coefficient of variation (COV). It is found that the MPH, MVPH, MPHLC and MPHCC method predictions are, in average, very close to each other, within 2% or less (median ratio between 0.98 and 1.02 for all method pairs). Therefore any of the four variations of those prismatic hull methods could be used interchangeably. For 3D, 4D and 5D histories (not shown in Table 1), the agreement is also very good among all prismatic hull methods, since their generated predictions are within 3% or less. For a history path with dimension dim , it is also verified that $1 \leq \lambda_{MPHLC} \leq \lambda_{MPHCC} \leq \lambda_{MPH} \leq \sqrt{dim}$. Therefore, the MPHCC results in Mises ratios slightly closer

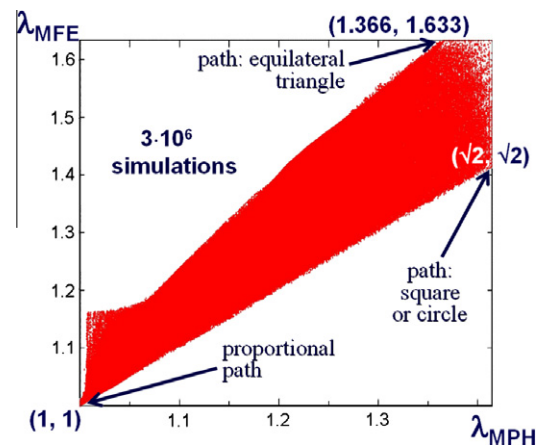


Fig. 6. Comparison between the λ ratios predicted by the MPH and MFE methods for 3×10^6 Monte-Carlo simulations with random 2D history paths.

Table 1
Median values of the ratios $\lambda_{row}/\lambda_{column}$ between the λ ratios calculated using the enclosing surface models shown in each row and column from the table, estimated from $3 \cdot 10^6$ Monte Carlo simulations for 2D history paths. The values in parentheses are the coefficient of variation (COV) of such ratios/correlations.

Row/col	MPHLC	MPHCC	MPH	MVPH	MFE	MVE	MB	MCE
MPHLC	–	1.00 (0.9%)	0.98 (2.3%)	1.00 (3.4%)	0.91 (5.9%)	0.84 (7.7%)	1.06 (6.2%)	0.87 (8.8%)
MPHCC	1.00 (0.9%)	–	0.98 (2.1%)	1.00(3.2%)	0.91 (5.7%)	0.84 (7.7%)	1.06 (6.3%)	0.87 (8.6%)
MPH	1.02 (2.3%)	1.02 (2.2%)	–	1.01 (1.9%)	0.93 (4.3%)	0.86 (6.6%)	1.09 (6.9%)	0.88 (7.0%)
MVPH	1.00(3.5%)	1.00(3.3%)	0.99 (1.8%)	–	0.91 (4.3%)	0.85 (6.7%)	1.07(7.8%)	0.86 (6.8%)
MFE	1.10 (5.9%)	1.10 (5.7%)	1.08 (4.3%)	1.10 (4.3%)	–	0.95 (6.5%)	1.18 (10.4%)	0.97 (4.1%)
MVE	1.19 (7.7%)	1.19 (7.7%)	1.16 (6.8%)	1.17 (6.9%)	1.05 (7.7%)	–	1.28 (8.8%)	1.00 (9.2%)
MB	0.94 (5.7%)	0.94 (5.8%)	0.92 (6.6%)	0.93 (7.4%)	0.85 (10.2%)	0.78 (9.6%)	–	0.80 (12.9%)
MCE	1.15 (8.7%)	1.15 (8.6%)	1.13 (6.9%)	1.16 (6.4%)	1.03 (4.5%)	1.00 (7.6%)	1.25 (12.2%)	–

Table 2
Fatigue life N (in cycles) experimentally measured and predicted using the Smith–Watson–Topper damage model and the Moment Of Inertia (MOI), Minimum Ball (MB) and Maximum Prismatic Hull (MPH) methods. Note that Cases 1–4 consider 2 cycles per block (e.g. the measured life for Case 1 was 1400 loading blocks, and thus shown as 2800 cycles).

Path/ N	experim.	MOI	MB	MPH
Case0	7100	7085	7085	7085
Case 1	2800	3379	3379	1150 ^a
Case 2	4200	4462	4462	1504 ^a
Case 3	820	640	640	229 ^a
Case 4	900	858	858	304 ^a
Case 5	3200	3557	3557	3557
Case 6	2600	2332	2393	2177
Case 7	1700	1590	1751	1453
Case 8	470	604	856 ^b	572
Case 9	660	604	856 ^b	572
Case 10	320	329	949 ^b	329
Case 11	1200	1073	2241 ^b	1073
Case 12	710	689	2023 ^b	689

^a As if 90° out of phase.

^b As if proportional.

to the MPH predictions than the MPHLC. In addition, it is also confirmed that $1 \leq \lambda_{MVPH} \leq \lambda_{MPH} \leq \sqrt{dim}$. Note that the lower bound 1 is obtained for proportional paths, while the upper bound \sqrt{dim} is associated with square or circular-shaped 2D paths ($dim = 2$) or higher-dimensional paths covering most of the surface of cubes, spheres, hypercubes or hyperspheres (for $3 \leq dim \leq 5$). Despite the relatively good agreement between the MVPH and other prismatic hull methods, with a maximum COV of 3.5%, it can underestimate the λ ratio by as much as 10% for nearly proportional histories.

Fig. 6 compares the MPH and MFE methods in 2D. Even though these methods seem coherent in the graph, they can lead to very different λ predictions. It is found that $\lambda_{MFE} \geq \lambda_{MPH}$ and, in average, λ_{MPH} is about 92.9% of λ_{MFE} (with a median ratio 0.93) with a COV of 4.3%. Similar conclusions are found for 3D, 4D and 5D histories. Note that the point $(\lambda_{MPH}, \lambda_{MFE}) = (0.5 + \sqrt{3}/2 \cong 1.366, 2\sqrt{2}/\sqrt{3} \cong 1.633)$ in the graph denotes the notable case of a path with the shape of an equilateral triangle. This significant difference between λ predictions suggests that a loading path shaped like an equilateral triangle in deviatoric space would provide a very good discriminant experiment to compare the adequacy of the MPH and MFE methods for a certain material.

From the Monte Carlo simulations with 2D paths it is also found that the MVE and MCE methods can severely overestimate λ , in special for almost proportional paths. As discussed before, almost proportional paths can lead to overly elongated ellipses in the MVE method, which can have a small area but an unrealistically large F-norm, leading to λ_{MVE} values larger than 2.0 in a few extreme cases, instead of the expected $\lambda = 1.0$. In addition, an almost proportional history defined by, e.g., a rectangular path with very low aspect ratio, would have an expected λ close to 1.0 (since it

is an almost proportional history), however the MCE method would circumscribe a circle (instead of an elongated ellipse) to such elongated rectangular path, wrongfully predicting $\lambda_{MCE} = \sqrt{2}$. An almost proportional triangular path would also result in $\lambda_{MCE} = \sqrt{2}$, revealing the inadequacy of the MCE method for such paths. Compared to the four prismatic hull methods, both MVE and MCE overestimate λ in average by 13–19% (median ratios 1.13–1.19), with a COV of up to 8.7%. Similar conclusions are found for 3D, 4D and 5D histories.

Finally, it is found that the MB method can severely underestimate λ in 2D paths, except for almost proportional load histories (where $\lambda \cong 1.0$). Good discriminant experiments to confirm the differences between the MB method and, e.g., the MFE method could make use of a square or circular path, where $(\lambda_{MFE}, \lambda_{MB}) = (\sqrt{2}, 1)$, or else of a path shaped as an equilateral triangle, where $(\lambda_{MFE}, \lambda_{MB}) = (2\sqrt{2}/\sqrt{3} \cong 1.633, 2/\sqrt{3} \cong 1.155)$. Both cases would result in $\lambda_{MFE}/\lambda_{MB} = \sqrt{2}$, a 41% difference that could be easily verified experimentally. Similar conclusions are found for 3D, 4D and 5D histories.

6. Experimental evaluation of the MOI and enclosing surface predictions

The MOI and enclosing surface estimates of effective ranges are now used to predict (in fact, to reproduce) the multiaxial fatigue lives of 304 stainless steel specimens tested by Itoh et al. [3]. Thirteen periodic histories are studied, represented by the block loadings shown in Fig. 7 for Cases 0 through 12. The multiaxial fatigue lives are calculated using the Smith–Watson–Topper (SWT) model in Bannantine–Socie's critical plane approach [1], searching for the plane where the damage parameter $\sigma_{max}\Delta\epsilon/2$ is maximized. The material properties used in these calculations are:

$$\epsilon = \frac{\sigma}{E} + \left(\frac{\sigma}{1754}\right)^{1/0.276}$$

$$\left(\sigma_{max} \frac{\Delta\epsilon}{2}\right)_{max} = \frac{757^2}{E} (2N)^{2b} + 30.5 \cdot (2N)^{b+c} \quad (17)$$

$$E = 197,000 \text{ MPa}, \quad b = -0.0886, \quad c = -0.303$$

Table 2 shows the experimental fatigue lives and the associated MOI, MB and MPH method predictions for each of the 13 loading histories. Note that the MOI method considers two cycles per block for Cases 1–4; this number of cycles can be deterministically obtained using the Modified Wang–Brown rainflow algorithm described in Part II of this paper.

The MOI method predicts that Cases 0–5 are proportional, since their $\lambda_{MOI} = 1.0$. This is reasonable, because the star and cross-shaped histories from Cases 1–4 are indeed the combination of two perpendicular proportional paths. These two perpendicular paths should not be considered as a single NP path, since they will most likely induce fatigue damage independently from each other in two perpendicular material planes. The MPH generates overly conservative predictions in these cases, since such enclosing

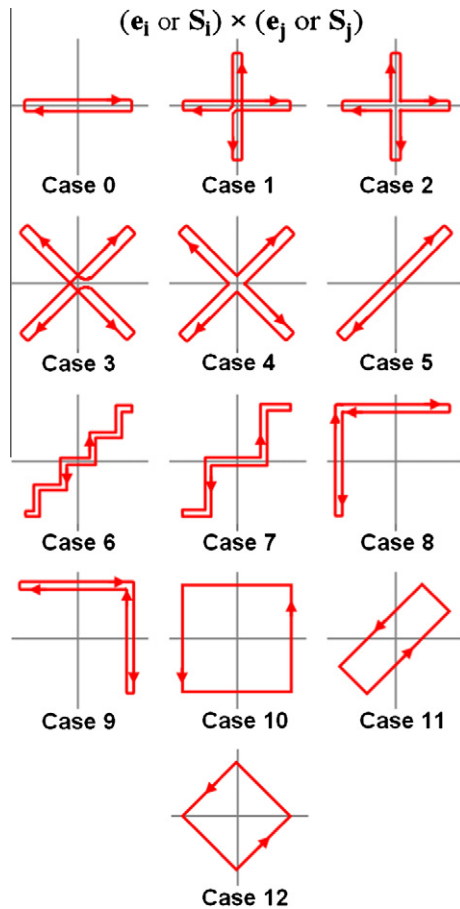


Fig. 7. History paths used in the experimental validation of the equivalent range predictions.

surface method would not be able to distinguish e.g. between a cross-shaped and a circular history, wrongfully estimating $\lambda_{MPH} = \sqrt{2}$ for both cases.

For Cases 5–12, the MOI method also predicts λ very well, agreeing with the MPH predictions. However, the MB method implicitly assumes that all 13 cases are proportional, since their $\lambda_{MB} = 1$, leading to poor predictions for Cases 8–12.

As expected from the quality of the λ ratio predictions, the MOI method results in quite reasonable life predictions in all studied histories, within only 20% from the experimental results. Note that these are **not** curve fittings, they really are true predictions made using the MOI method (together with the SWT model for critical planes) without any adjustable parameter. The MPH method, on the other hand, gives poor life predictions for Cases 1–4, since it wrongfully assumes (through $\lambda_{MPH} = \sqrt{2}$) that these cross or star-shaped histories are 90° out-of-phase, instead of being proportional. And the MB method results in non-conservative predictions in Cases 8–12, since it wrongfully assumes (through $\lambda_{MB} = 1$) that these paths are proportional.

7. Conclusions

In this work, all enclosing surface methods from the literature were reviewed and compared, and new methods were proposed. The conclusions from the simulations and experiments are:

1. the prismatic hull methods MPHLC and MPHCC are very similar to the MPH and MVPH methods, but with a much simpler search algorithm for 3D to 5D histories;
2. the only recommended ellipsoid hull is the Minimum F-norm Ellipsoid (MFE), which results in similar (but not identical) λ predictions when compared to the prismatic hull methods;
3. the Minimum Circumscribed Ellipsoid (MCE) and Minimum Volume Ellipsoid (MVE) methods may overestimate the equivalent stress (or strain) ranges, in special for triangular or rectangular-shaped nearly-proportional paths, leading to conservative life predictions;
4. the Minimum Ball (MB) method usually underestimates the equivalent stress (or strain) ranges in NP histories, resulting in non-conservative predictions;
5. experimental results demonstrated the effectiveness of the proposed MOI method for all studied cases, accounting for the contribution of every single segment of the loading path and thus dealing with an arbitrarily shaped history without losing information about such shape, as an enclosing surface method would.

In summary, the Minimum F-norm Ellipsoid and all four Maximum Prismatic Hull (MPH) models are efficient to predict equivalent amplitudes in NP histories, even though they overestimate it for cross or star-shaped paths. However, from a philosophical point of view, it is difficult to justify that an enclosing surface that does not represent well the mean component of a path could be used to calculate an equivalent stress or strain range. This is even more difficult to justify when the path has a very odd shape. The MOI method, on the other hand, can effectively calculate all these quantities even for complex-shaped paths, without the need for adjustable parameters.

Finally, note that, for non-periodic histories, or for periodic histories consisting of blocks with more than 1 cycle, it is necessary to perform a multiaxial rainflow count of the history before applying the MOI method to obtain the effective ranges. This rainflow count is described in Part II of this paper. The resulting half cycles are combined, if possible, into full cycles, and then the MOI method (or any enclosing surface method) is applied to each counted cycle (or half-cycle) to obtain the effective stress or strain range and associated damage. The damage calculated for each cycle is then combined using Miner's linear damage accumulation rule.

References

- [1] Socie DF, Marquis GB. Multiaxial fatigue. SAE; 1999.
- [2] Deperrois A. Sur le calcul des limites d'endurance des aciers. Thèse de Doctorat. Ecole Polytechnique, Paris; 1991.
- [3] Kida S, Itoh T, Sakane M, Ohnami M, Socie DF. Dislocation structure and non-proportional hardening of type 304 stainless steel. *Fatigue Fract Eng Mater Struct* 1997;20(10):1375–86.
- [4] Shamsaei N, Fatemi A, Socie DF. Multiaxial cyclic deformation and non-proportional hardening employing discriminating load paths. *Int J Plast* 2010;26(12):1680–701.
- [5] Sines G. Behavior of metals under complex static and alternating stresses. Metal fatigue. McGraw-Hill; 1959.
- [6] Crossland B. Effect of large hydrostatic pressures on the torsional fatigue strength of an alloy steel. In: Proceedings of international conference on fatigue of metals. London: IMechE; 1956. p. 138–49.
- [7] Findley WN. A theory for the effect of mean stress on fatigue of metals under combined torsion and axial load or bending. *J Eng Ind* 1959;301–6.
- [8] McDiarmid DL. A shear stress based critical-plane criterion of multiaxial fatigue failure for design and life prediction. *Fatigue Fract Eng Mater Struct* 1994;7(12):1475–85.
- [9] Brown M, Miller KJ. A theory for fatigue under multiaxial stress-strain conditions. *Inst Mech Eng* 1973;187:745–56.
- [10] Fatemi A, Socie DF. A critical plane approach to multiaxial damage including out-of-phase loading. *Fatigue Fract Eng Mater Struct* 1988;11:149–66.
- [11] Smith RN, Watson P, Topper TH. A stress-strain parameter for the fatigue of metals. *J Mater* 1970;5(4):767–78.
- [12] Langlais TE, Vogel JH, Chase TR. Multiaxial cycle counting for critical plane methods. *Int J Fatigue* 2003;25:641–7.
- [13] Kachanov M. On the concept of damage in creep and in the brittle-elastic range. *Int J Damage Mech* 1994;3:329–37.
- [14] Dang Van K. Macro-micro approach in high-cycle multiaxial fatigue. ASTM STP 1191, ASTM; 1993.

- [15] Dang Van K, Papadopoulos IV. High-cycle metal fatigue. Springer; 1999.
- [16] Freitas M, Li B, Santos JLT. Multiaxial fatigue and deformation: testing and prediction. ASTM STP 1387; 2000.
- [17] Gonçalves CA, Araújo JA, Mamiya EN. Multiaxial fatigue: a stress based criterion for hard metals. *Int J Fatigue* 2005;27:177–87.
- [18] Zouain N, Mamiya EN, Comes F. Using enclosing ellipsoids in multiaxial fatigue strength criteria. *Eur J Mech – A Solids* 2006;25:51–71.
- [19] Mamiya EN, Araújo JA, Castro FC. Prismatic hull: a new measure of shear stress amplitude in multiaxial high cycle fatigue. *Int J Fatigue* 2009;31:1144–53.
- [20] Iliouchine AA. Plasticité, Éditions Eyrolles, Paris; 1956.
- [21] Bishop JE. Characterizing the non-proportional and out-of-phase extend of tensor paths. *Fatigue Fract Eng Mater Struct* 2000;23:1019–32.
- [22] Papadopoulos IV, Davoli P, Gorla C, Filippini M, Bernasconi A. A comparative study of multiaxial high-cycle fatigue criteria for metals. *Int J Fatigue* 1997;19:219–35.
- [23] Bernasconi A. Efficient algorithms for calculation of shear stress amplitude and amplitude of the second invariant of the stress deviator in fatigue criteria applications. *Int J Fatigue* 2002;24(6):649–57.
- [24] Ballard P, Dang Van K, Deperrois A, Papadopoulos IV. High cycle fatigue and a finite element analysis. *Fatigue Fract Eng Mater Struct* 1994;18(3):397–411.
- [25] Castro FC, Araújo JA, Mamiya EN, Zouain N. Remarks on multiaxial fatigue limit criteria based on prismatic hulls and ellipsoids. *Int J Fatigue* 2009;31:1875–81.